Planning throwing motions for mobile manipulators

Gravina, Giovanbattista   Nunziante, Luca

March 2023

Abstract

The aim of this project is to plan a throwing motion for a planar mobile manipulator (MM), in an attempt to increase its workspace or reduce the time needed for a pick and place task. The motion planning problem is formulated as an Optimal Control Problem (OCP) and solved using numerical optimization via the Optimization Toolbox of MATLAB. Robot balance is guaranteed along the whole planned trajectory using an appropriate nonlinear constraint based on the MM full dynamics, ensuring non-negative moments around the edges of the support polygon. A first set of simulations show the results obtained via different approaches to the optimization framework, and then aggressive manoeuvres are analyzed.

1 Introduction

Mobile manipulators are robotic systems that consist of a mobile base and a manipulator arm. Thanks to their versatility they are effectively used in various areas such as logistics, due to to their augmented workspace, and disaster response since they combine high dexterity and mobility and can be designed to traverse hazardous environments. However, one of the main challenges in designing MMs is achieving balance: due to their structure, the center of gravity and the ZMP of the system constantly change as the robot moves, and this clearly affects the robot stability, leading to a possible tip over and potential damage to the system or harm to the environment and people around it.

Research in planning throwing motion is practically motivated, since this kind of dynamic manipulation can increase the working range and shorten an operation cycle time. Although finding a throwing state (joints position and velocity) for a MM is a non-injective problem, estimating a kinodynamically feasible throwing trajectory that also satisfies the balance constraint is not trivial. Moreover, when dealing with arbitrary objects one should also consider that the grasp of the object, its mass distribution and aerodynamics heavily influence its trajectory. This has been successfully addressed with model-free methods [5]. In this work we will consider to throw a ball modeled as a point mass, neglecting its rotation. This implies that after its release, the ball will experience planar ballistic flight, as in [1].

Another approach to throwing problems is using sampling based methods as in [6], where they sample a state that sends the object on a ballistic arc to the target, and reach it via probabilistic bidirectional planners from the initial and final state, naturally dividing the task in a throwing and stopping phase.

Generation of throwing motion has also been formulated as an OCP [2]: in optimal control theory, the fields of optimization and automatic control are combined to compute optimal control inputs to the system that is being controlled. In general, a local solution to a Non Linear Program (NLP)[1] is found using iterative schemes. The major difference between different iterative solvers is how the search direction and step length are computed. When computing local solutions to general NLPs, there are mainly two families of optimization methods that are used: Sequential Quadratic Programming (SQP) methods and nonlinear Interior-Point (IP) methods — in this work the former will be used.

We investigate various approaches to the NLP formulation and the respective results are shown in the simulations. Comparisons on the planned throwing trajectories are carried out, analyzing for each motion: relevant robot configurations, ZMP position, velocities and control inputs profiles. Finally, we further discuss the influence of the balance constraint by performing aggressive maneuvers.

The following work is organized as follows. The considered problem is formulated in Section 2. In Section 3 the dynamic model of the mobile manipulator (MM) is presented, along with the equations of motion and the balance criterion. In Section 4 the approaches to solve the motion planning problem are detailed. Some simulations are presented in Section 5, and finally some concluding remarks are offered in Section 6.

2 Problem formulation

Consider a mobile manipulator operating in a 2-dimensional (vertical) workspace $\mathcal{W}$, that is required to transport an object from an initial to a final goal position $\boldsymbol{p}_{goal}$. We consider a case in which the robot is unable to reach the intended final position due to structural limitations (e.g. obstacles blocking the path) or it is desirable to reduce the time of the operation. For this reason, the robot is called to release the object from a distance, rather than delivering it to the intended goal.

Ballistic motion We assume the thrown object follows a planar ballistic trajectory. Given a world frame $\mathcal{F}_w$ as in Fig. 1, the equations that describe the object motion are

$$\begin{cases} x(t) = & \dot{x}_0 t + x_0 \\ z(t) = & \dot{z}_0 t - \frac{1}{2} g t^2 + z_0 \end{cases} \tag{1}$$

[1]A NLP is an optimization problem where at least one of the involved functions is nonlinear.

where $\boldsymbol{p}_0 = (x_0, z_0)$ is the position of the point-mass object at the initial instant of the ballistic motion and $\dot{\boldsymbol{p}}_0 = (\dot{x}_0, \dot{z}_0)$ is its velocity; $g = 9.81\ m/s^2$ is the gravity acceleration and t is the time variable. Assuming, without loss of generality, that the desired final object position lies on the ground, i.e., $\boldsymbol{p}_{goal} = (x_{goal}, 0)$, from (1) we can write

$$-x_{goal} + x_0 + \frac{\dot{x}_0 \dot{z}_0}{g} + \dot{x}_0 \sqrt{\frac{\dot{z}_0^2}{g^2} + \frac{2z_0}{g}} = 0 \tag{2}$$

Assuming that at time instant t_{init} the robot is in its initial configuration $\boldsymbol{q}_{init}$ at rest with the object attached to its end-effector, we wish to plan a motion that:

R1: starts from the robot initial state $\boldsymbol{x}_{init} = (\boldsymbol{q}_{init}, \boldsymbol{0})$ and ends to a final resting state $\boldsymbol{x}_{final}$ at time t_{final}, while it is such that there exists a time instant $t_{rel} \in [t_{init}, t_{final}]$ at which, if released, the object can reach its goal position $\boldsymbol{p}_{goal}$;

R2: is kinodynamically feasible, in the sense that it is consistent with the robot dynamic model and respects existing constraints on joint and velocity limits and input torque bounds;

R3: preserves the robot balance, i.e., all wheels maintain contact with the ground.

3 Modeling

We consider a planar (vertical) MM consisting of one driving wheel and two caster wheels, as reported in Fig. 1, and a 2R manipulator mounted on top. For the actuated wheel we assume no slippage, thanks to the wheel-ground friction, while the two caster wheels only contribute to the robot balance. Moreover, we assume all of them to be in point contact with the ground. Being a fully planar problem, the mobile base can only move forward and backward, i.e. it is not subject to any non-holonomic constraint.

Following [4], to represent the pose of the mobile base we use 3 fictitious joints that connect the world frame $\mathcal{F}_w$ to a frame attached to the point of contact of the driving wheel of the robot with the ground ($\mathcal{F}_2$ in Fig. 1). The fictitious joints are arranged with the first two being prismatic and along the world axes x_w, z_w and a revolute one along y_w, as depicted in Fig. 1. So, the robot configuration is $\boldsymbol{q} = (x_b, z_b, \theta_y, q_1, q_2) \in \mathbb{R}^5$ where the first three components represent the base pose, and the last two the arm configuration.
To derive the dynamic model of this MM, we take the Lagrangian approach [3] and compute the positions and velocities of the Center of Mass (CoM) of each body using the Denavit-Hartenberg (DH) frames of Fig. 1, and the associated Table 1.

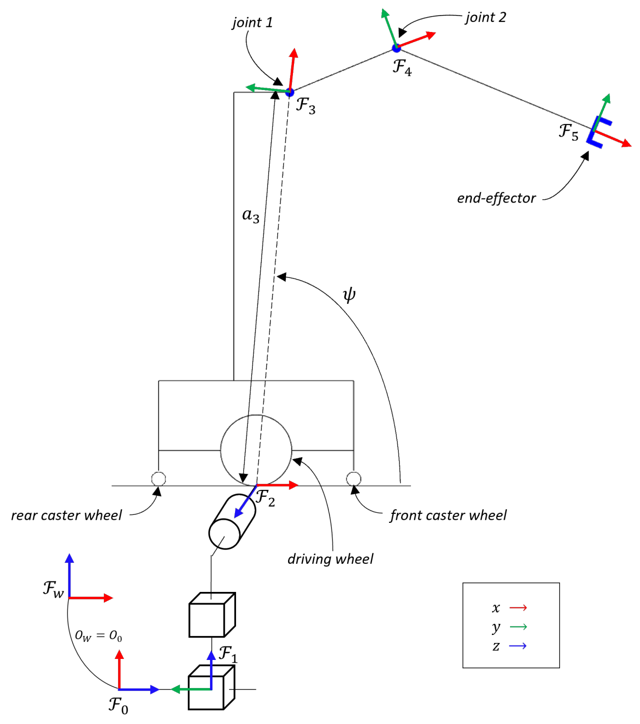

Figure 1: DH frames attached to the robot to derive its dynamic model.

The obtained robot dynamics is

$$\boldsymbol{B}(\boldsymbol{q})\ddot{\boldsymbol{q}} + \boldsymbol{n}(\boldsymbol{q}, \dot{\boldsymbol{q}}) = \boldsymbol{S}(\boldsymbol{q})\boldsymbol{u} + \boldsymbol{A}(\boldsymbol{q})\boldsymbol{\lambda} \tag{3}$$

where $\boldsymbol{B}(\boldsymbol{q}) \in \mathbb{R}^{5\times5}$ is the inertia matrix, $\boldsymbol{n}(\boldsymbol{q}, \dot{\boldsymbol{q}}) \in \mathbb{R}^5$ encompasses the Coriolis, centrifugal and gravitational terms, $\boldsymbol{S}(\boldsymbol{q}) \in \mathbb{R}^{5\times3}$ is the matrix that maps the control inputs $\boldsymbol{u} \in \mathbb{R}^3$ to forces performing work on the generalized coordinates, and the matrix $\boldsymbol{A}(\boldsymbol{q}) \in \mathbb{R}^{5\times2}$ is used to express at the generalized coordinates level the contact forces $\boldsymbol{\lambda} \in \mathbb{R}^2$.

In the case under consideration:

- $\boldsymbol{S}(\boldsymbol{q})$ is constant, and since the inputs $\boldsymbol{u}$ are the torque of the wheel and of the two manipulator joints, it is

$$\boldsymbol{S} = \begin{bmatrix} \frac{1}{r_w} & 0 & 0 \\ 0 & 0 & 0 \\ 0 & 0 & 0 \\ 0 & 1 & 0 \\ 0 & 0 & 1 \end{bmatrix}$$

  where r_w is the driving wheel radius.

i	a_i	α_i	d_i	θ_i
1	0	$-\pi/2$	x_b	$-\pi/2$
2	0	$\pi/2$	z_b	$-\pi/2$
3	a_3	0	0	$\theta_y + \psi$
4	h_1	0	0	$q_1 - \psi$
5	h_2	0	0	q_2

Table 1: DH table associated to the frames in Fig. 1 where h_1 and h_2 are the manipulator link lengths.

- due to the robot motion on the horizontal ground, the coordinates z_b, θ_y — associated to the second and third fictitious joints — are constrained to a constant value (zero for the choice of θ_3 in Table 1), therefore $\boldsymbol{h}(\boldsymbol{q}) = \begin{pmatrix} z_b \\ \theta_y \end{pmatrix} = \boldsymbol{0}$ and $\boldsymbol{A}(\boldsymbol{q}) = (\frac{\partial \boldsymbol{h}}{\partial \boldsymbol{q}})^T \in \mathbb{R}^{5\times 2}$.

3.1 Equations of motion

We can split $\boldsymbol{q}$ in $\boldsymbol{q}_f = (z_b, \theta_y)$ and $\boldsymbol{q}_r = (x_b, q_1, q_2)$ and have 2 selection matrices so that $\boldsymbol{q}_f = \boldsymbol{Q}_f \boldsymbol{q}$ and $\boldsymbol{q}_r = \boldsymbol{Q}_r \boldsymbol{q}$. Since $\ddot{\boldsymbol{q}}_f = \boldsymbol{0}$ it is $\ddot{\boldsymbol{q}} = \boldsymbol{Q}_r^T \ddot{\boldsymbol{q}}_r$, and by left-multiplying (3) by $\boldsymbol{Q}_r$ we have

$$\boldsymbol{Q}_r \boldsymbol{B}(\boldsymbol{q}) \boldsymbol{Q}_r^T \ddot{\boldsymbol{q}}_r + \boldsymbol{Q}_r \boldsymbol{n}(\boldsymbol{q}, \dot{\boldsymbol{q}}) = \boldsymbol{Q}_r \boldsymbol{S}(\boldsymbol{q}) \boldsymbol{u} \tag{4}$$

Note that in our work $\boldsymbol{Q}_r \boldsymbol{A}(\boldsymbol{q}) \boldsymbol{\lambda} = \boldsymbol{0}$ since $\boldsymbol{h}(\boldsymbol{q})$ does not depend on $\boldsymbol{q}_r$.

Starting from (4) and with some manipulation — following [3] — we can derive the robot state space model. Indeed, it is particularly simple in our case due to the absence of non-holonomic constraints. Given the state $\boldsymbol{x} = (\boldsymbol{q}_r, \dot{\boldsymbol{q}}_r)$, we have

$$\dot{\boldsymbol{x}} = \boldsymbol{\phi}(\boldsymbol{x}, \boldsymbol{u}) = \begin{pmatrix} \dot{\boldsymbol{q}}_r \\ \boldsymbol{M}^{-1}(\boldsymbol{q})(\boldsymbol{E}\boldsymbol{u} - \boldsymbol{m}(\boldsymbol{q}, \dot{\boldsymbol{q}})) \end{pmatrix} \tag{5}$$

where

$$\begin{aligned} \boldsymbol{M}(\boldsymbol{q}) &= \boldsymbol{Q}_r \boldsymbol{B}(\boldsymbol{q}) \boldsymbol{Q}_r^T \ , \\ \boldsymbol{m}(\boldsymbol{q}, \dot{\boldsymbol{q}}) &= \boldsymbol{Q}_r \boldsymbol{n}(\boldsymbol{q}, \dot{\boldsymbol{q}}) \ , \\ \boldsymbol{E} &= \boldsymbol{Q}_r \boldsymbol{S} \ . \end{aligned}$$

3.2 Contact forces

To analyze the robot balance, it is sufficient to know the sum of the forces orthogonal to the ground and the moments parallel to the ground that the robot exerts.

Left multiplying (3) by $\boldsymbol{Q}_f$ we get

$$\boldsymbol{Q}_f \boldsymbol{B}(\boldsymbol{q}) \boldsymbol{Q}_r^T \ddot{\boldsymbol{q}}_r + \boldsymbol{Q}_f \boldsymbol{n}(\boldsymbol{q}, \dot{\boldsymbol{q}}) = \boldsymbol{\lambda} \tag{6}$$

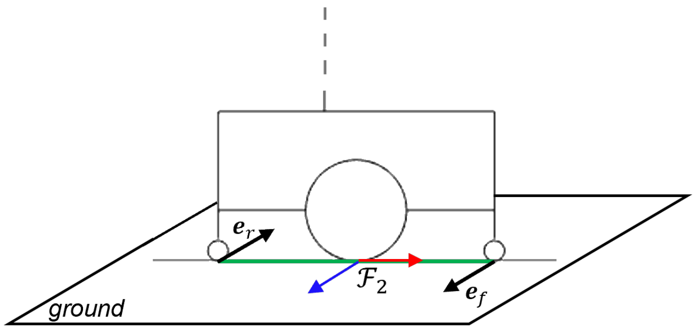

Figure 2: In green the robot support polygon.

where $\boldsymbol{Q}_f \boldsymbol{S}(\boldsymbol{q})\boldsymbol{u} = \boldsymbol{0}$ since the control torques do not perform work on $\boldsymbol{q}_f$. Note that $\boldsymbol{Q}_f \boldsymbol{A}(\boldsymbol{q})$ in (6) is the identity matrix, hence $\boldsymbol{\lambda}$ represents the contact force and moment along the axes of the second and third fictitious joints.

Let f_{f_2}, μ_{f_3} be the force and moment that the robot exerts along the z-axis of frame $\mathcal{F}_1, \mathcal{F}_2$ respectively (see Fig. 1), then

$$\begin{pmatrix} f_{f_2} \\ \mu_{f_3} \end{pmatrix} = -\boldsymbol{\lambda} \; . \tag{7}$$

Given the expression of $\ddot{\boldsymbol{q}}_r$ from (5), we can plug it in (6) and get f_{f_2}, μ_{f_3} as function of the state and inputs, i.e.

$$\begin{aligned} \begin{pmatrix} f_{f_2} \\ \mu_{f_3} \end{pmatrix} = &- \boldsymbol{Q}_f \boldsymbol{B}(\boldsymbol{q}) \boldsymbol{Q}_r^T \boldsymbol{M}^{-1}(\boldsymbol{q}) \boldsymbol{E} \boldsymbol{u} \\ &+ \boldsymbol{Q}_f \boldsymbol{B}(\boldsymbol{q}) \boldsymbol{Q}_r^T \boldsymbol{M}^{-1}(\boldsymbol{q}) \boldsymbol{m}(\boldsymbol{q}, \dot{\boldsymbol{q}}) \\ &- \boldsymbol{Q}_f \boldsymbol{n}(\boldsymbol{q}, \dot{\boldsymbol{q}}) \; . \end{aligned} \tag{8}$$

Then, we consider the orthogonal to the ground force and parallel to ground moment exerted by the robot at the origin of $\mathcal{F}_2$ and express them in $\mathcal{F}_2$ as

$$\begin{aligned} {}^2\boldsymbol{f} = \boldsymbol{f} &= {}^2\boldsymbol{R}_w(\boldsymbol{q}) f_{f_2} {}^w\hat{\boldsymbol{z}}_1 \\ {}^2\boldsymbol{\mu} = \boldsymbol{\mu} &= {}^2\boldsymbol{R}_w(\boldsymbol{q}) \mu_{f_3} {}^w\hat{\boldsymbol{z}}_2 \end{aligned} \tag{9}$$

where ${}^2\boldsymbol{R}_w(\boldsymbol{q})$ is the rotation matrix of $\mathcal{F}_2$ w.r.t. $\mathcal{F}_w$, and ${}^w\hat{\boldsymbol{z}}_1, {}^w\hat{\boldsymbol{z}}_2$ are the unit vectors of the z-axis of $\mathcal{F}_1$ and $\mathcal{F}_2$ expressed in $\mathcal{F}_w$.

3.3 Balance constraint

The evaluation of the robot balance is done considering the moments applied by the robot around the support polygon edges: balance is preserved if the resulting moments are non-negative.

Being a 2-dimensional problem, the support polygon reduces to the segment joining the contact points of the two caster wheels, and the two edges collapse into the contact points of the rear and front wheel, as shown in Fig. 2.

We express in $\mathcal{F}_2$ two unit vectors $\boldsymbol{e}_r$, $\boldsymbol{e}_f$ orthogonal to the motion plane, and denote their starting point — the passive wheel contact points with the ground — as $\boldsymbol{p}_r$, $\boldsymbol{p}_f$. Then, the balance criterion is expressed as

$$\begin{aligned} \mu_r &= \boldsymbol{e}_r^T(-\boldsymbol{p}_r \times \boldsymbol{f} + \boldsymbol{\mu}) \geq 0 \ , \\ \mu_f &= \boldsymbol{e}_f^T(-\boldsymbol{p}_f \times \boldsymbol{f} + \boldsymbol{\mu}) \geq 0 \ . \end{aligned} \tag{10}$$

where all the vectors are expressed in $\mathcal{F}_2$. From (8), (9) it is possible to notice that μ_r, μ_f are function of the robot state and control input. Indeed, substituting (8) in (9), and then plugging the result in (10), we can derive the balance constraint

$$\boldsymbol{b}(\boldsymbol{x}, \boldsymbol{u}) \geq \boldsymbol{0} \tag{11}$$

Zero Moment Point computation Since (11) is equivalent to constraining the ZMP to be inside the support polygon [4], in the simulations we will check the position of the ZMP. Writing the static equilibrium with all the vectors expressed in $\mathcal{F}_2$, we have

$$\begin{aligned} \boldsymbol{s} + \boldsymbol{f} &= \boldsymbol{0} \\ \boldsymbol{p}_{zmp} \times \boldsymbol{s} + \boldsymbol{\mu} &= \boldsymbol{0} \end{aligned} \tag{12}$$

where $\boldsymbol{s}$ is the ground reaction force, and $\boldsymbol{p}_{zmp}$ is the position vector of the ZMP. From (12), since in our planar case it is $\boldsymbol{\mu} \perp \boldsymbol{f} \perp \boldsymbol{p}_{zmp}$, we get

$$\boldsymbol{p}_{zmp} = \begin{pmatrix} \frac{\mu_z}{f_y} \\ 0 \\ 0 \end{pmatrix} \tag{13}$$

where μ_z, f_y are respectively the z and y component of $\boldsymbol{\mu}$, $\boldsymbol{f}$, which also are the only non-zero components of these vectors.

4 Proposed method

When planning a throwing trajectory for a robot, the motion is divided into two main phases: the *throwing phase* that takes place in the time interval $[t_{init}, t_{rel}]$ and the *stopping phase* in $(t_{rel}, t_{final}]$. The robot first has to arrive at instant t_{rel} at an appropriate throwing state $\boldsymbol{x}_{rel}$, release the object to be thrown, and then it enters the stopping phase where it must decelerate reaching a resting state $\boldsymbol{x}_{final}$ at instant t_{final}. Dividing the motion in two phases, we need to ensure continuity on the state when they are addressed separately.

To solve the motion planning problem we take different approaches:

- (**Approach 0**) solve an OCP to find a kinematically feasible throwing state $\boldsymbol{x}_{rel}$. Then, we solve the two phases separately: one OCP gives an optimal trajectory from $\boldsymbol{x}_{init}$ to $\boldsymbol{x}_{rel}$, and another OCP from $\boldsymbol{x}_{rel}$ to $\boldsymbol{x}_{final}$. The optimal trajectories satisfy R2, R3.
- (**Approach 1**) optimization of the throwing state is incorporated in the same OCP of the throwing phase trajectory, while the stopping phase is solved separately with a second OCP.
- (**Approach 2**) the throwing phase, the throwing state and the stopping phase are incorporated in the same OCP.

Note that the final stopping configuration is never specified, only the final velocity is required to be zero.

4.1 Approach 0

Step 1 Find a kinematically feasible throwing state $\boldsymbol{x}_{rel}$ solving the following NLP

$$\boldsymbol{x}_{rel} = \underset{\boldsymbol{x}}{\operatorname{argmin}}\, \dot{\boldsymbol{q}}_r^T \boldsymbol{W} \dot{\boldsymbol{q}}_r \tag{14a}$$

subject to:

$$\boldsymbol{x}_{min} \leq \boldsymbol{x} \leq \boldsymbol{x}_{max} \tag{14b}$$

$$\textit{ballistic constraint} \tag{14c}$$

where (14b) constrains the solution to satisfy the state bounds, and $\boldsymbol{W}$ is a suitably chosen weighting matrix to equally weight the contribution to the norm of each component of $\dot{\boldsymbol{q}}_r$. Indeed, the first joint velocity (m/s) is dimensionally different than the other two (rad/s).

Ballistic constraint To derive the ballistic constraint (14c) as function of the state of the robot $\boldsymbol{x}$, it is sufficient to note that in (1), (2) the position $\boldsymbol{p}_0$ and velocity $\dot{\boldsymbol{p}}_0$ of the object at the starting instant of its ballistic motion coincide with the end-effector position and velocity at the throwing instant t_{rel}. We can express the direct and differential kinematics of the robot in the form

$$\boldsymbol{p}_{ee} = \boldsymbol{\sigma}(\boldsymbol{q}_r) \ , \ \dot{\boldsymbol{p}}_{ee} = \boldsymbol{J}(\boldsymbol{q}_r)\dot{\boldsymbol{q}}_r \tag{15}$$

where $\boldsymbol{\sigma}(\cdot)$ is the function that maps the joint coordinates of the robot to the end-effector position, and $\boldsymbol{J}(\boldsymbol{q}_r) = \frac{\partial \boldsymbol{\sigma}}{\partial \boldsymbol{q}_r} \in \mathbb{R}^{2\times 3}$ is the end-effector jacobian. Then, substituting (15) in (2) we obtain the (scalar) ballistic constraint as function of the robot state in the form

$$g(\boldsymbol{x}) = 0 \tag{16}$$

Step 2 Solve the throwing phase by formulating another NLP: let the duration of the throwing phase be $T_t = t_{rel} - t_{init}$ and the sampling time δ, we end up with $N_t = T_t/\delta$ control intervals, and the decision variables $\boldsymbol{w}_t$ are

$$\boldsymbol{w}_t = \begin{bmatrix} \boldsymbol{x}_0^T \ \boldsymbol{u}_0^T \ \boldsymbol{x}_1^T \ \boldsymbol{u}_1^T \ \dots \ \boldsymbol{x}_{N_t-1}^T \ \boldsymbol{u}_{N_t-1}^T \ \boldsymbol{x}_{N_t}^T \end{bmatrix}^T \in \mathbb{R}^{9N_t+6} \tag{17}$$

where $\boldsymbol{x}_i, \boldsymbol{u}_i$ are the robot state and inputs at the *i-th* control instant, and the subscript t is used to point out that the variables refer to the throwing phase. The NLP can now be formulated as

$$\min_{\boldsymbol{w}_t} \sum_{i=0}^{N_t-1} (\dot{\boldsymbol{q}}_{r,i}^T \boldsymbol{W} \dot{\boldsymbol{q}}_{r,i} + \boldsymbol{u}_i^T \boldsymbol{R} \boldsymbol{u}_i) + \dot{\boldsymbol{q}}_{r,N_t}^T \boldsymbol{W} \dot{\boldsymbol{q}}_{r,N_t} \tag{18a}$$

subject to:

$$\boldsymbol{x}_{i+1} - \boldsymbol{\phi}_{d\text{-}t}^l(\boldsymbol{x}_i, \boldsymbol{u}_i) = \mathbf{0} \quad i = 0 \dots N_t - 1 \tag{18b}$$

$$\boldsymbol{x}_0 - \boldsymbol{x}_{init} = \mathbf{0} \tag{18c}$$

$$\boldsymbol{x}_{N_t} - \boldsymbol{x}_{rel} = \mathbf{0} \tag{18d}$$

$$\boldsymbol{x}_{min} \leq \boldsymbol{x}_i \leq \boldsymbol{x}_{max} \quad i = 0 \dots N_t \tag{18e}$$

$$\boldsymbol{u}_{min} \leq \boldsymbol{u}_i \leq \boldsymbol{u}_{max} \quad i = 0 \dots N_t - 1 \tag{18f}$$

$$\boldsymbol{b}^l(\boldsymbol{x}_i, \boldsymbol{u}_i) \geq \mathbf{0} \quad i = 0 \dots N_t - 1 \ . \tag{18g}$$

The cost function is composed of three terms: we have the running and terminal cost associated to the joint velocity $\dot{\boldsymbol{q}}_r$ that are damping terms, and the cost associated to the control effort with its weighting matrix $\boldsymbol{R}$. In the constraints, $\boldsymbol{\phi}_{d\text{-}t}^l(\cdot,\cdot)$ is the discrete-time dynamics obtained with the 4th order Runge-Kutta integration method; the superscript l indicates that we are considering the robot dynamics with the load attached to the end-effector; in (18d) we constrain the last state of phase one $\boldsymbol{x}_{N_t}$ to be $\boldsymbol{x}_{rel}$, solution of the NLP (14); $\boldsymbol{x}_{init}$ is a resting initial state; the constraints (18b), (18e), (18f), (18g) make the solution satisfy the requirements R2 and R3 specified in Section 2.

Step 3 To address the stopping phase we formulate another NLP. Let the duration of the stopping time be $T_s = t_{final} - t_{rel}$, and $N_s = T_s/\delta$, the decision variables now are

$$\boldsymbol{w}_s = \begin{bmatrix} \boldsymbol{x}_0^T \ \boldsymbol{u}_0^T \ \boldsymbol{x}_1^T \ \boldsymbol{u}_1^T \ \dots \ \boldsymbol{x}_{N_s-1}^T \ \boldsymbol{u}_{N_s-1}^T \ \boldsymbol{x}_{N_s}^T \end{bmatrix}^T \in \mathbb{R}^{9N_s+6} \tag{19}$$

where the subscript s points out that we are addressing the stopping phase. The NLP is formulated as

$$\min_{\boldsymbol{w}_s} \sum_{i=0}^{N_s-1} (\dot{\boldsymbol{q}}_{r,i}^T \boldsymbol{W} \dot{\boldsymbol{q}}_{r,i} + \boldsymbol{u}_i^T \boldsymbol{R} \boldsymbol{u}_i) + \dot{\boldsymbol{q}}_{r,N_s}^T \boldsymbol{W} \dot{\boldsymbol{q}}_{r,N_s} \tag{20a}$$

subject to:

$$\boldsymbol{x}_{i+1} - \boldsymbol{\phi}_{d\text{-}t}(\boldsymbol{x}_i, \boldsymbol{u}_i) = \boldsymbol{0} \quad i = 0 \ldots N_s - 1 \tag{20b}$$

$$\boldsymbol{x}_0 - \boldsymbol{x}_{rel} = \boldsymbol{0} \tag{20c}$$

$$\dot{\boldsymbol{q}}_{r,N_s} = \boldsymbol{0} \tag{20d}$$

$$\boldsymbol{x}_{min} \leq \boldsymbol{x}_i \leq \boldsymbol{x}_{max} \quad i = 0 \ldots N_s \tag{20e}$$

$$\boldsymbol{u}_{min} \leq \boldsymbol{u}_i \leq \boldsymbol{u}_{max} \quad i = 0 \ldots N_s - 1 \tag{20f}$$

$$\boldsymbol{b}(\boldsymbol{x}_i, \boldsymbol{u}_i) \geq \boldsymbol{0} \quad i = 0 \ldots N_s - 1 \ . \tag{20g}$$

where $\boldsymbol{\phi}_{d\text{-}t}(\cdot, \cdot)$ is the robot dynamics without a payload, (20c) assures continuity on the state between the two phases, and (20d) constrains the final velocity to be zero. Note that (18g) is different from (20g) since the robot dynamics differ, as the payload is not attached to the end-effector anymore.

4.2 Approach 1

Differently from before, within this approach, we only have 2 NLPs to solve.

Step 1 Formulate an NLP that addresses the throwing phase, including the optimization of $\boldsymbol{x}_{rel}$ since we no longer make use of a previous pure kinematic optimization. The decision variables are

$$\boldsymbol{w}_t = \begin{bmatrix} \boldsymbol{x}_0^T & \boldsymbol{u}_0^T & \boldsymbol{x}_1^T & \boldsymbol{u}_1^T & \ldots & \boldsymbol{x}_{N_t-1}^T & \boldsymbol{u}_{N_t-1}^T & \boldsymbol{x}_{N_t}^T \end{bmatrix}^T \in \mathbb{R}^{9N_t+6} \tag{21}$$

and the optimization is formulated as

$$\min_{\boldsymbol{w}_t} \sum_{i=0}^{N_t-1} (\dot{\boldsymbol{q}}_{r,i}^T \boldsymbol{W} \dot{\boldsymbol{q}}_{r,i} + x_{b,i}^2 \rho + \boldsymbol{u}_i^T \boldsymbol{R} \boldsymbol{u}_i) + \dot{\boldsymbol{q}}_{r,N_t}^T \boldsymbol{W} \dot{\boldsymbol{q}}_{r,N_t} \tag{22a}$$

subject to:

$$\boldsymbol{x}_{i+1} - \boldsymbol{\phi}_{d\text{-}t}^l(\boldsymbol{x}_i, \boldsymbol{u}_i) = \boldsymbol{0} \quad i = 0 \ldots N_t - 1 \tag{22b}$$

$$\boldsymbol{x}_0 - \boldsymbol{x}_{init} = \boldsymbol{0} \tag{22c}$$

$$g(\boldsymbol{x}_{N_t}) = 0 \tag{22d}$$

$$\boldsymbol{x}_{min} \leq \boldsymbol{x}_i \leq \boldsymbol{x}_{max} \quad i = 0 \ldots N_t \tag{22e}$$

$$\boldsymbol{u}_{min} \leq \boldsymbol{u}_i \leq \boldsymbol{u}_{max} \quad i = 0 \ldots N_t - 1 \tag{22f}$$

$$\boldsymbol{b}^l(\boldsymbol{x}_i, \boldsymbol{u}_i) \geq \boldsymbol{0} \quad i = 0 \ldots N_t - 1 \tag{22g}$$

where again $\boldsymbol{x}_{init}$ is a resting initial state, (22g) assures balance throughout the motion, $x_{b,i}$ is x_b (defined in Section 3) in the *i-th* control instant, and the related term in the cost function with weight $\rho \in \mathbb{R}$ penalizes the distance of the robot base from the origin. This term leads to a solution where the robot throws the object limiting base movements towards the goal[2]. Note how the constraint (22d) is different from (18d), as it does not rely on a previous optimization. This allows for more flexibility and a bigger throwing range.

Step 2 The second NLP simply solves the stopping phase: the decision variables are

$$\boldsymbol{w}_s = \begin{bmatrix} \boldsymbol{x}_0^T \; \boldsymbol{u}_0^T \; \boldsymbol{x}_1^T \; \boldsymbol{u}_1^T \; \dots \; \boldsymbol{x}_{N_s-1}^T \; \boldsymbol{u}_{N_s-1}^T \; \boldsymbol{x}_{N_s}^T \end{bmatrix}^T \in \mathbb{R}^{9N_s+6} \tag{23}$$

and the NLP is formulated as

$$\min_{\boldsymbol{w}_s} \sum_{i=0}^{N_s-1} (\dot{\boldsymbol{q}}_{r,i}^T \boldsymbol{W} \dot{\boldsymbol{q}}_{r,i} + x_{b,i}^2 \rho + \boldsymbol{u}_i^T \boldsymbol{R} \boldsymbol{u}_i) + \dot{\boldsymbol{q}}_{r,N_s}^T \boldsymbol{W} \dot{\boldsymbol{q}}_{r,N_s} \tag{24a}$$

subject to:

$$\boldsymbol{x}_{i+1} - \boldsymbol{\phi}_{d\text{-}t}(\boldsymbol{x}_i, \boldsymbol{u}_i) = \boldsymbol{0} \quad i = 0 \dots N_s - 1 \tag{24b}$$

$$\boldsymbol{x}_0 - \boldsymbol{x}_{rel} = \boldsymbol{0} \tag{24c}$$

$$\dot{\boldsymbol{q}}_{r,N_s} = \boldsymbol{0} \tag{24d}$$

$$\boldsymbol{x}_{min} \leq \boldsymbol{x}_i \leq \boldsymbol{x}_{max} \quad i = 0 \dots N_s \tag{24e}$$

$$\boldsymbol{u}_{min} \leq \boldsymbol{u}_i \leq \boldsymbol{u}_{max} \quad i = 0 \dots N_s - 1 \tag{24f}$$

$$\boldsymbol{b}(\boldsymbol{x}_i, \boldsymbol{u}_i) \geq \boldsymbol{0} \quad i = 0 \dots N_s - 1 \tag{24g}$$

where $\boldsymbol{x}_{rel}$ is the final state of the solution to (22).

4.3 Approach 2

This is the most straightforward approach, as a single NLP is solved. The control intervals are $N = (T_t + T_s)/\delta$, hence the decision variables are

$$\boldsymbol{w} = \begin{bmatrix} \boldsymbol{x}_0^T \; \boldsymbol{u}_0^T \; \boldsymbol{x}_1^T \; \boldsymbol{u}_1^T \; \dots \; \boldsymbol{x}_{N-1}^T \; \boldsymbol{u}_{N-1}^T \; \boldsymbol{x}_N^T \end{bmatrix}^T \in \mathbb{R}^{9N+6} \tag{25}$$

[2]Note that in (18) this was not needed as the throwing state was fixed.

and the NLP is formulated as

$$\min_{\boldsymbol{w}} \sum_{i=0}^{N-1} (\dot{\boldsymbol{q}}_{r,i}^T \boldsymbol{W} \dot{\boldsymbol{q}}_{r,i} + x_{b,i}^2 \rho + \boldsymbol{u}_i^T \boldsymbol{R} \boldsymbol{u}_i) + \dot{\boldsymbol{q}}_{r,N}^T \boldsymbol{W} \dot{\boldsymbol{q}}_{r,N} \tag{26a}$$

subject to:

$$\boldsymbol{x}_{i+1} - \boldsymbol{\phi}_{d\text{-}t}^l(\boldsymbol{x}_i, \boldsymbol{u}_i) = \boldsymbol{0} \quad i = 0 \dots k-1 \tag{26b}$$

$$\boldsymbol{x}_{i+1} - \boldsymbol{\phi}_{d\text{-}t}(\boldsymbol{x}_i, \boldsymbol{u}_i) = \boldsymbol{0} \quad i = k \dots N-1 \tag{26c}$$

$$g(\boldsymbol{x}_k) = 0 \tag{26d}$$

$$\boldsymbol{x}_0 - \boldsymbol{x}_{init} = \boldsymbol{0} \tag{26e}$$

$$\dot{\boldsymbol{q}}_{r,N} = \boldsymbol{0} \tag{26f}$$

$$\boldsymbol{x}_{min} \leq \boldsymbol{x}_i \leq \boldsymbol{x}_{max} \quad i = 0 \dots N \tag{26g}$$

$$\boldsymbol{u}_{min} \leq \boldsymbol{u}_i \leq \boldsymbol{u}_{max} \quad i = 0 \dots N-1 \tag{26h}$$

$$\boldsymbol{b}^l(\boldsymbol{x}_i, \boldsymbol{u}_i) \geq \boldsymbol{0} \quad i = 0 \dots k-1 \tag{26i}$$

$$\boldsymbol{b}(\boldsymbol{x}_i, \boldsymbol{u}_i) \geq \boldsymbol{0} \quad i = k \dots N-1 \tag{26j}$$

where $k = T_t/\delta$ is the index that identifies the throwing instant.

5 Simulations

In this section we present simulations using the different introduced Approaches. In every experiment we intend to throw a ball of 3 kg and, if not otherwise specified, we have the following parameters

$$T_t = 1 \ s \ , \qquad T_s = 1.25 \ s \ , \qquad \delta = 0.025 \ s \ , \tag{27a}$$

$$\boldsymbol{W} = diag(\left[\tfrac{1}{h_1 h_2}, \ 1, \ 1\right]) \ , \qquad \boldsymbol{R} = \boldsymbol{I}_3 \ , \qquad \rho = 5 \ . \tag{27b}$$

where h_1, h_2 are the manipulator link lengths, and $\boldsymbol{I}_3 \in \mathbb{R}^{3\times 3}$ is the identity matrix. With these choices, we have $N_t = 40$ and $N_s = 50$. As a result, the decision variables are $\boldsymbol{w}_t \in \mathbb{R}^{366}$, $\boldsymbol{w}_s \in \mathbb{R}^{456}$, and $\boldsymbol{w} \in \mathbb{R}^{816}$.

Moreover, unless otherwise specified, we choose the following joint position and velocity limits, and input torque bounds:

$$0 \leq x_b < +\infty \ [m] \ , \qquad -\frac{\pi}{4} \leq q_1 \leq \frac{9}{10}\pi \ [rad] \ , \qquad -\frac{\pi}{4} \leq q_2 \leq \frac{\pi}{2} \ [rad] \tag{28a}$$

$$|\dot{x}_b| \leq 0.9998 \ [m/s] \ , \qquad |\dot{q}_1| \leq 5 \ [rad/s] \ , \qquad |\dot{q}_2| \leq 5 \ [rad/s] \tag{28b}$$

$$|u_w| \leq 6 \ [Nm] \ , \qquad |u_1| \leq 39 \ [Nm] \ , \qquad |u_2| \leq 39 \ [Nm]. \tag{28c}$$

where the joint position limits allow the robot the widest possible range of motion while avoiding self-collision.

In order to make a fair comparison among the different approaches, the simulations in Sections 5.1, 5.2, 5.3 share the same resting initial configuration $\boldsymbol{q}_{r,0} = (9.3647, \ 1.4062, \ \pi/2) \ [m, rad, rad]$. We examine the maximum reachable x_{goal}, found with a resolution of 0.1 m, given $\boldsymbol{x}_{init}$, the parameters (27) and the bounds (28). Videos of these experiments are available at this link.

5.1 Approach 0

As previously said, here three NLPs are solved, namely (14), (18), (20). Note that if we use (28a) in (14), the solution to that NLP is simply dropping the ball at the goal due to the unboundedness of x_b. Hence, to force a throwing configuration, only for (14) we set $0 \leq x_b \leq 10 - d_b/2$ where d_b is the width of the base.

The throwing range achievable with this methodology is very limited: the maximum x_{goal} is 11.9 m, and the throwing configuration obtained solving (14) is shown in Fig. 3b. This limited goal is due to breaking the robot motion in three optimization schemes: considering further goals, Step 1 optimization (14) is able to find a solution $\boldsymbol{x}_{rel}$, but Step 2 fails. Indeed, it is not guaranteed that (18) returns a feasible solution since it may not be possible to go from $\boldsymbol{x}_{init}$ to $\boldsymbol{x}_{rel}$ given the robot dynamics and the time budget T_t. For this reason, in Approach 1 we decide to add $\boldsymbol{x}_{rel}$ in the same optimization scheme as the throwing phase.

Finally, we also report the joint positions, velocities, control inputs and the ZMP position during the whole motion in Fig. 4.

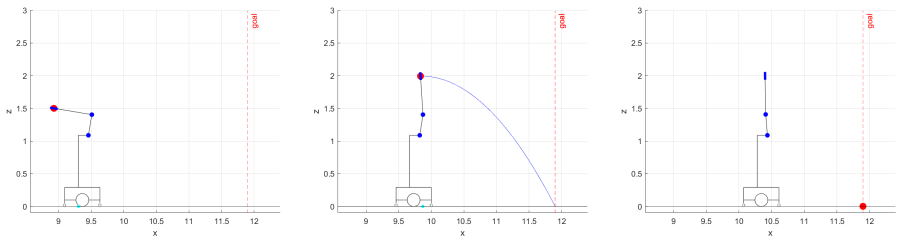

(a) Initial configuration (b) Throwing configuration (c) Stopping configuration

Figure 3: Relevant robot configurations during the throwing motion found with Approach 0. The ball (in red) is released from the configuration in (b) with a velocity $\boldsymbol{v} = (3.2243,\ 0.0284)$ $[m/s]$ and its time of flight is $T_f = 0.6404$ s. The obtained throwing range is of 2.0648 m. The cyan marker in (a) and (b) is the ZMP, and it is not present in (c) as we do not have a control input at instant t_{final}.

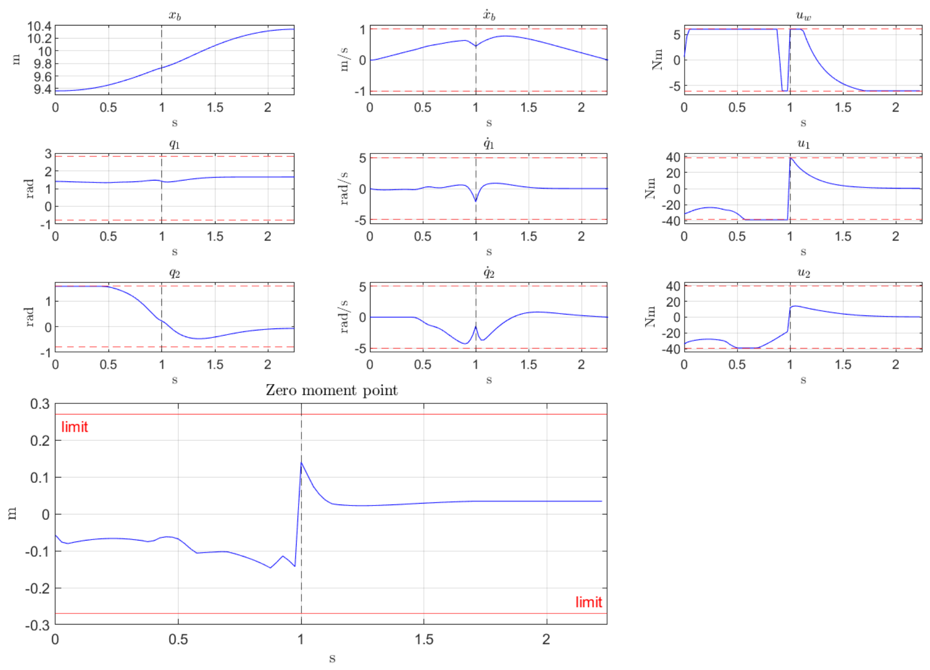

Figure 4: Joints data and ZMP profile for the experiment done with Approach 0. The ZMP profile is one dimensional since the support polygon (see Fig. 2) is a line. The black vertical dashed line reported in all the plots identifies the throwing instant t_{rel}.

5.2 Approach 1

Finding $\boldsymbol{x}_{rel}$ and the phase one trajectory in a single optimization gives this approach more flexibility w.r.t. Approach 0. Indeed, it is possible to increase x_{goal} up to 13 m and the found throwing state (see Fig. 5b) is very different from the one in Fig. 3b.

However, we still address the stopping phase in a different optimization scheme w.r.t the throwing phase. So, a similar problem as before may arise: even when (22) finds a solution, it is not guaranteed that the robot is able to stop in the allotted time T_s. To address this issue, in approach 2 we incorporate everything in the same optimization scheme.

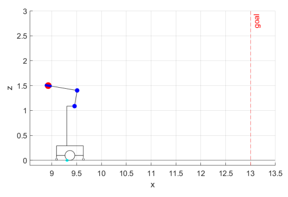
(a) Initial configuration

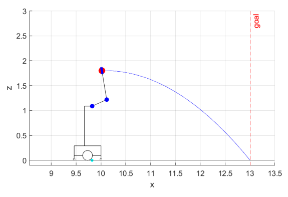
(b) Throwing configuration

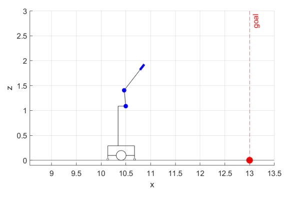
(c) Stopping configuration

Figure 5: Relevant robot configurations during the throwing motion found with Approach 1. The ball (in red) is released from the configuration in (b) with a velocity $\boldsymbol{v} = (4.8297,\ 0.11)\ [m/s]$ and its time of flight is $T_f = 0.6174\ s$. The obtained throwing range is $2.9817m$. The cyan marker in (a) and (b) is the ZMP, and it is not present in (c) as we do not have a control input at instant t_{final}.

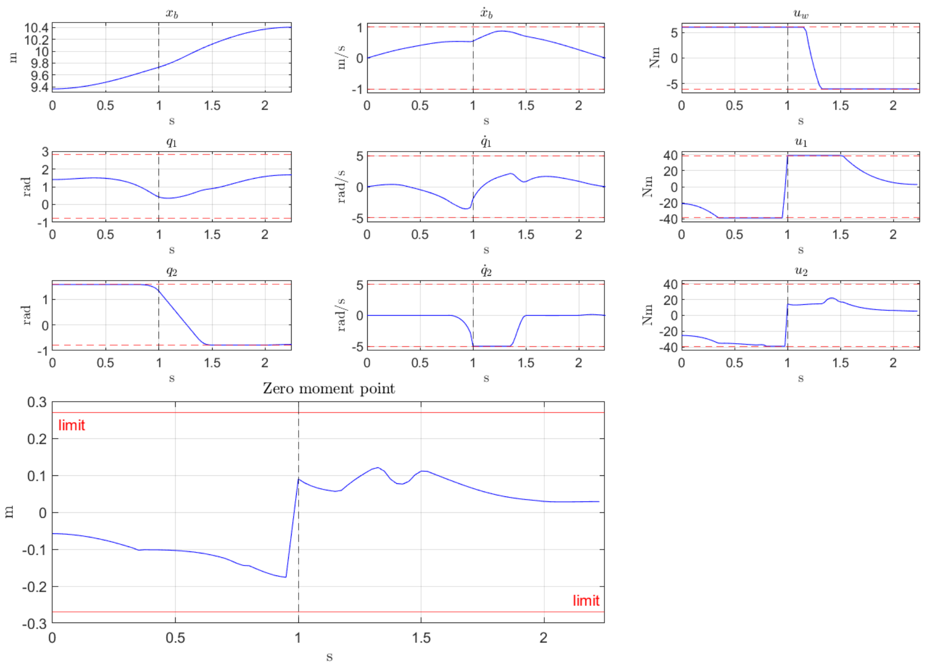

Figure 6: Joints data and ZMP profile for the experiment done with Approach 1. The ZMP profile is one dimensional since the support polygon (see Fig. 2) is a line. The black vertical dashed line reported in all the plots identifies the throwing instant t_{rel}.

5.3 Approach 2

This approach can be seen as a collapse of the previous one as here only (26) is solved. Indeed, the same maximum goal of the previous approach is the best we can do.

However, here the control effort of $u_1,\ u_2$ during the stopping phase is reduced (see Fig. 8). This is the effect of integrating in a single optimization scheme both the throwing and stopping phase. Indeed, with this approach the optimization variables during the stopping phase are affected by the during throwing: this leads to an overall better solution, as expected.

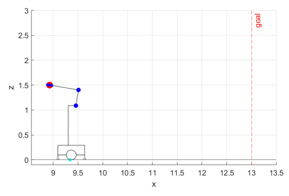
(a) Initial configuration

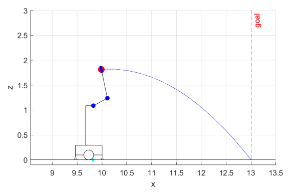
(b) Throwing configuration

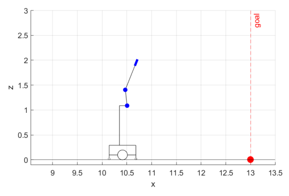
(c) Stopping configuration

Figure 7: Relevant robot configurations during the throwing motion found with approach 2. The ball is released from the configuration in (b) with a velocity $\boldsymbol{v} = (4.6793,\ 0.3393)\ [m/s]$ and its time of flight is $T_f = 0.6439\ s$. The achieved throwing range is 3.013 m. The cyan marker in (a) and (b) is the ZMP. It is not present in (c) as we do not have a control input at instant t_{final}.

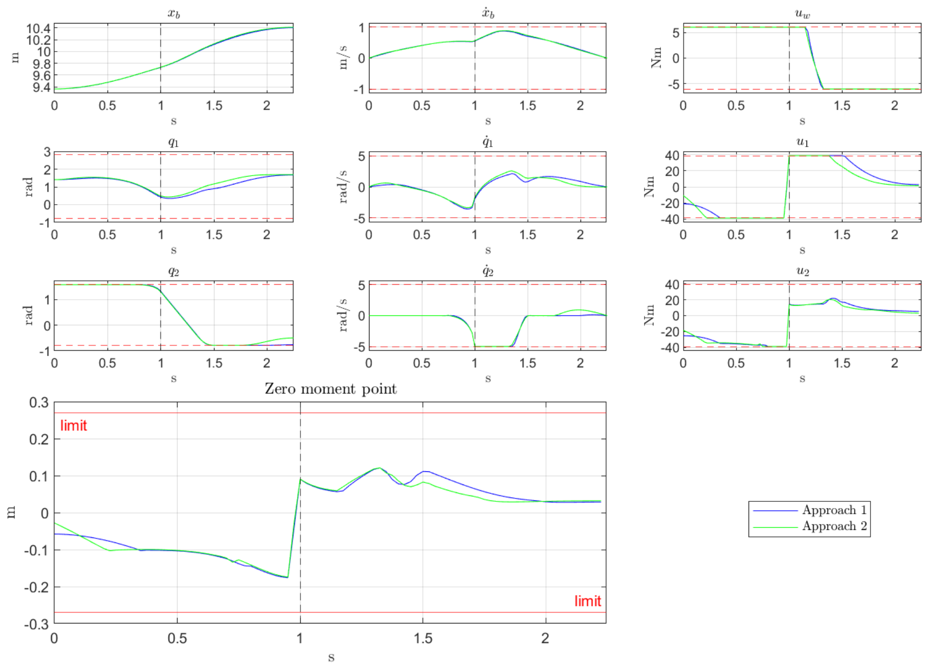

Figure 8: Joints data and ZMP profile for the experiment done with Approach 1 (in blue) and Approach 2 (in green). The ZMP profile is one dimensional since the support polygon (see Fig. 2) is a segment. The black vertical dashed line reported in all the plots identifies the throwing instant t_{rel}.

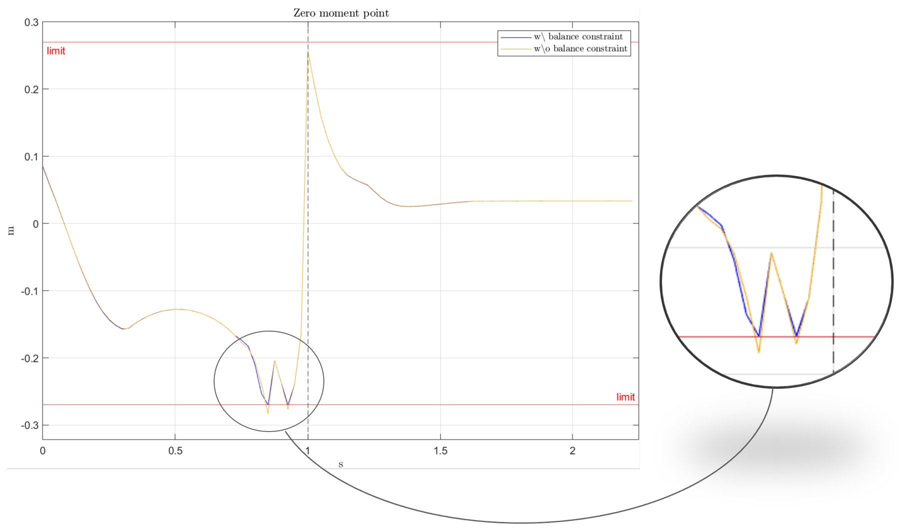

Figure 9: ZMP profile with torque bounds (29), integrating the balance constraint in the optimization (blue) and removing it (orange). In the latter case we see the ZMP exceeds the bounds, i.e. the robot falls.

5.4 Approach 2: increase torque bounds

One thing shared between the three reported simulations is that the balance constraint is inactive since the ZMPs in Fig. 4, 6, 8 are far from the bounds. Indeed, removing the constraint from all the NLPs still yields balance-safe trajectories. To clearly see the influence of the balance criterion, the control input bounds are updated as follows

$$|u_w| \leq 6 \ [Nm] \ , \ |u_1| \leq 70 \ [Nm] \ , \ |u_2| \leq 70 \ [Nm] \ . \tag{29}$$

These new bounds were found via several trials with various torque combinations, and this choice was the one that made the balance constraint active with the least modifications to the original bounds (28c) on $|u_1|, |u_2|$.

Indeed, starting from the same initial configuration and using the input bounds (29), the goal can be increased up to 14.6 m, and from Fig. 9 it is possible to see that without balance constraint the robot would fall, while integrating it in the optimization yields a balance-safe trajectory.

5.5 Approach 2: aggressive manoeuvres

All the results offered in this section are obtained with bounds (28a), (28b), (29) and the throwing time is updated to $T_t = 2\ s$. Moreover, one may argue that the initial configuration considered so far is clearly intended for throwing and not a generic one. For this reason, other simulations are analyzed with different initial configurations. These changes are done to show more aggressive and dynamic motions, to better appreciate the importance of the balance constraint.

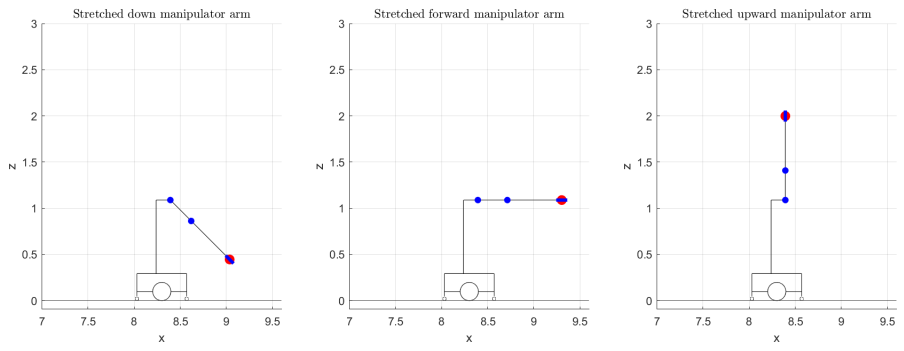
Stretched down manipulator arm
Stretched forward manipulator arm
Stretched upward manipulator arm
z
x

(a) $\boldsymbol{q}_r = (8.3,\ -\pi/4,\ 0)$ (b) $\boldsymbol{q}_r = (8.3,\ 0,\ 0)$ (c) $\boldsymbol{q}_r = (8.3,\ \pi/2,\ 0)$

Figure 10: Representation of the initial configurations C1, C2, C3 and the respective joint coordinates value $\boldsymbol{q}_r$.

It is worth reporting that solving (26) is computationally expensive as its decision variables now are $\boldsymbol{w} \in \mathbb{R}^{1176}$. However, using as initial guess a previous solution with a slightly different $\boldsymbol{p}_{goal}$ reduces the computation time by a factor of 4. The simulations we carried out involve three different initial configurations:

C1: stretched down manipulator arm;

C2: stretched forward manipulator arm;

C3: stretched upward manipulator arm.

Moreover, the influence of the parameter ρ is investigated analyzing, for each of the three cases, two scenarios

S1: set $\rho = 5$ in (26);

S2: set $\rho = 1000$ in (26), assigning high importance to the robot base distance from the origin;

However, results show that simulations sharing the same $\boldsymbol{p}_{goal}$ only differ in how they reach the throwing state (that is similar in the three cases). Hence, for the sake of clarity, we here focus solely on C1 (see Fig. 10a) as it is a more likely initial state for a pick-and-place task, but the same considerations can be done also for the other cases.

Videos of all the experiments — including the ones using C2, C3 — are available at this link.

5.5.1 Stretched down arm

The starting configuration is shown in Fig. 10a where we highlight that q_1 is at its lower position limit. In Fig. 11 are reported the resulting relevant robot configurations associated to S1, S2.

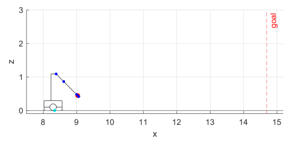

(a) Initial configuration

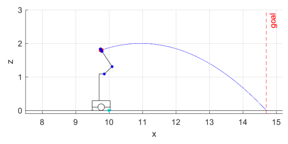

(b) Throwing configuration

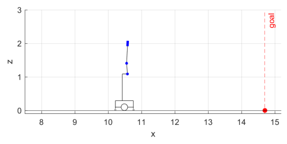

(c) Stopping configuration

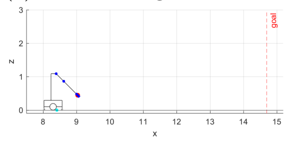

(d) Initial configuration

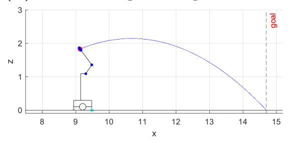

(e) Throwing configuration

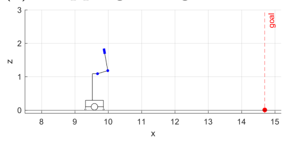

(f) Stopping configuration

Figure 11: Relevant configurations of the simulations starting with the stretched down arm. The first and second row refer to the planned trajectories with S1 and S2 respectively. The cyan marker in (a),(b), (d) and (e) is the ZMP, and it is not present in (c) and (f) as we do not have a control input at instant t_{final}.

As expected, a direct comparison between the throwing configurations — respectively in Fig. 11b, 11e — shows that a higher penalization of the base motion in scenario S2 allows the object to be released at a greater distance from the goal position, with a difference of 0.5532 m. This is also reflected in the stopping phase as the robot is able to shorten its stopping distance of 0.3433 m (see Fig. 11c, 11f and the top left plot in Fig. 12). Thus, the whole distance covered by the robot base is reduced of 0.8965 m, corresponding to about 41%.

A further analysis of the stopping configurations in Fig. 11 shows a clear difference: in S2 the robot stops in a configuration quite different from the almost stretched up one, reached in S1. A possible motivation is that weighting more the base motion term results in a decrease in the relevance of control effort minimization in the cost function, as confirmed by the torques profile in Fig. 12.

Fig. 12 also shows that the ZMP reaches the limits without exceeding them thanks to the presence of the balance constraint in the optimization scheme, hence the planned trajectory is balance-safe.

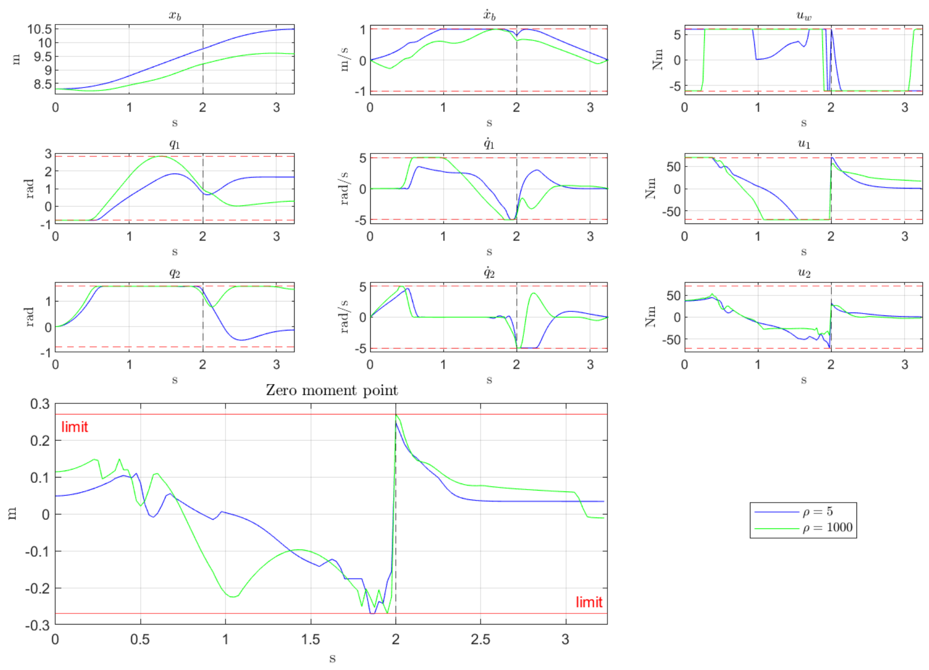

Figure 12: Joints data and ZMP profile for the experiment done starting with the arm down configuration in scenarios S1 (blue), S2 (green). The ZMP profile is one dimensional since the support polygon (see Fig. 2) is a segment. The black vertical dashed line reported in all the plots identifies the throwing instant t_{rel}.

6 Conclusions

In this work we have presented various approaches to address a throwing motion planning problem for a planar MM. To prevent the robot loss of balance in cases where it is called to execute aggressive motions we included a constraint that restricts the robot feasible motions to those that result to non-negative moments around the support polygon edges.

To study the throwing motion planning problem, we have tried different OCP formulations. Starting from Approach 0, we finally ended up with a single NLP able to generate balance-safe throwing motion. This last approach is general, and can be applied to any MM. It can also be easily extended to a real robot, where also an appropriate control scheme is needed to follow the planned motion.

Moreover, tuning of the weights in the NLP can yield motions with different specific attributes, as shown here with the base penalization term.

Finally, simulations showed that the used balance constraint can effectively handle aggressive manoeuvres where otherwise there would be a balance loss.

References

[1] Sergey A. Kolyubin and Anton S. Shiriaev. Planning longest pitch trajectories for compliant serial manipulators. In *2016 IEEE/RSJ International Conference on Intelligent Robots and Systems (IROS)*, pages 3150–3155, 2016.

[2] Ferenc Lombai and Gabor Szederkenyi. Throwing motion generation using nonlinear optimization on a 6-degree-of-freedom robot manipulator. In *2009 IEEE International Conference on Mechatronics*, pages 1–6, 2009.

[3] Bruno Siciliano, Lorenzo Sciavicco, Luigi Villani, and Giuseppe Oriolo. Robotics: Modelling, planning and control. 2008.

[4] Spyridon G. Tarantos and Giuseppe Oriolo. Real-time motion generation for mobile manipulators via NMPC with balance constraints. In *2022 30th Mediterranean Conference on Control and Automation (MED)*, pages 853–860, 2022.

[5] Andy Zeng, Shuran Song, Johnny Lee, Alberto Rodriguez, and Thomas Funkhouser. Tossingbot: Learning to throw arbitrary objects with residual physics, 2019.

[6] Yajia Zhang, Jingru Luo, and Kris Hauser. Sampling-based motion planning with dynamic intermediate state objectives: Application to throwing. In *2012 IEEE International Conference on Robotics and Automation*, pages 2551–2556, 2012.